2018-12-01

On site determination of trace metals in estuarine sediments by field-portable-XRF.

Turner, Andrew

10.1016/j.talanta.2018.08.024
Talanta
Elsevier

On site determination of trace metals in estuarine sediments by field-portable-XRF

Andrew Turner*, Alex Taylor

School of Geography, Earth and Environmental Sciences, Plymouth University, Drake Circus, Plymouth PL4 8AA, UK

*Corresponding author

e-mail: aturner@plymouth.ac.uk

doi.org/10.1016/j.talanta.2018.08.024
Accepted 6 August 2018
Embargoed until 6 August 2019

Abstract

A portable x-ray fluorescence (XRF) spectrometer and mobile test stand have been employed to examine the feasibility of measuring trace metals in estuarine sediment in the field. The instrument was able to detect the trace metals: As, Cr, Cu, Pb, Sn and Zn; and the geochemical proxy metals: Ca, Fe, K and Rb; in both fresh and freeze-dried surficial samples from the Tamar and Tavy estuaries, southwest England, that had been emplaced in polyethylene bags over the detector window. The presence of interstitial water in fresh samples acted as both a diluent of sediment mass and an attenuator of incident and fluorescent x-rays, resulting in measured (fresh weight) metal concentrations that were significantly lower than corresponding (dry weight) concentrations derived from dry analyses. Gravimetric correction for fractional water content (f_w ~ 0.2 to 0.6) gave rise to results that were within 20% of those derived from dry analyses with the exception of K, whose relatively low energy fluorescent x-rays were subject to significant attenuation from the aqueous medium; further x-ray attenuation was observed for both K and Ca through the sample bag, thereby limiting the usefulness of the approach for these metals. A relationship between the concentration of Rb and f_w in fresh samples suggests that Rb may be used as a proxy for interstitial water content through its covariance with sediment grain size. Accordingly, on site measurements of trace metals of sufficient fluorescent x-ray energies may be corrected empirically with respect to Rb in order to simultaneously account for variations in granulometry and mass contribution of water. On this basis, results from an axial transect of the Tamar and an intertidal transect in the Tavy were able to detect variations in trace metal concentrations that were consistent with known sources and geochemical behaviours.

Keywords: portable-XRF; estuarine sediments; trace metals; contaminants; on site

1. Introduction

Estuaries represent the river-ocean interface of the hydrosphere and play a key role in the transportation, modification and storage of materials and chemicals derived from natural erosion and anthropogenic inputs in the watershed (Regnier et al., 2014). Estuarine sediments are particularly significant vectors and reactors in this respect since they undergo considerable internal recycling through resuspension-deposition and provide a high surface area for the adsorption-desorption of a variety of chemicals (Turner and Millward, 2002). Trace metal(loid) contaminants, such as As, Cu, Pb and Zn, interact strongly with suspended and deposited estuarine sediment through a variety of processes, and concentrations in intertidal or subtidal deposits often provide an indication of the anthropogenic signature in the catchment (Kennish, 1998). Accordingly, measurements of trace metals in sediments form an integral component of many assessments of estuarine quality or status (Mucha et al., 2004; Azevedo et al., 2013; Cao et al., 2014).

Conventionally, metals and metalloids (hereafter referred to as metals) in estuarine and coastal sediments are determined by a suitable spectrophotometric technique following total or quasi-total digestion of dried samples by flux fusion or combined acid attack (Wei and Haraguchi, 1999; Zhao et al., 2017). Analysis by inductively coupled plasma spectrometry or atomic absorption spectrometry, for example, is rapid and relatively straightforward, but digestion may be time- and resource-intensive and can generate considerable quantities of hazardous waste. Alternative, non-destructive approaches for measuring metals in sediments include neutron activation analysis and benchtop x-ray fluorescence (XRF) spectrometry (Al-Jundi, 2001; Alyazichi et al., 2017) but equipment may be expensive to run and, regarding the former, access to a nuclear reactor is required. Moreover, both sample preparation, involving milling and pelletisation or packing, and sample analyses are time-consuming.

With the miniaturisation of x-ray tubes, improvements in detector resolution and advancements in signal processing capability, portable, energy-dispersive XRF has gained increasing use for the rapid, cost-effective and non-destructive analysis of metals in particulate geosolids over the past two decades (Radu and Diamond, 2009; Quiroz-Jiménez and Roy, 2017). Minimal sample processing (sieving and drying) has allowed a high throughput of samples in the laboratory, but measurements may also be performed in the field if material is sufficiently fine, homogeneous and dry (Higueros et al., 2012). In this respect, estuarine sediments are more challenging because of a relatively high content of interstitial water. Thus, besides the risk of damaging sensitive components within the detector window, water acts as a diluent of sediment mass and an attenuator of incident (primary) and fluorescent (secondary) x-ray, effects that reduce signal intensity and tend to underestimate true (absolute) concentrations.

Attempts have been made to measure metals in sediment samples in the fresh or part-dried state by portable XRF, in both the laboratory and in the field, with results deemed to be of sufficient quality to screen for heavy metal contamination or to aid decision-making for management purposes (Stallard et al., 1995; Kirtray et al., 1998; Ge et al., 2001; Lemiere et al., 2014; Mejía-Piña et al., 2017). However, the significance of water and suitable means for its correction are rarely addressed in a systematic or quantitative manner that allow absolute, dry weight concentrations to be accurately predicted. To this end, we evaluate the potential of a battery-powered Niton XRF instrument coupled with a mobile test stand for the field measurement of trace metals in estuarine sediments. Specifically, the effects of x-ray attenuation by suitable containers and by interstitial water are examined in controlled experiments in the laboratory, with results compared with those obtained from an optimised geometry whereby samples had been freeze-dried and milled prior to packing into

customised XRF sample cups. A configuration of the instrument and stand is tested in the field, with means of correcting on site results for water content explored which are based on gravimetric measures or the use of analyte proxies for moisture.

2. Materials and methods

2.1. XRF instrumentation and configuration

In the current study, samples were analysed for various metals either in the laboratory or in the field using a Niton XL3t 950 He GOLDD+ portable XRF spectrometer. Measurements were conducted in a 'mining' mode and with a beam width of 8 mm (equivalent to a measurement area of 50 mm^2) for a total time of 60 s, comprising successive counting periods of 30 s at 50 kV/40 μA (main filter), 15 s at 20 kV/100 μA (low filter) and 15 s at 50 kV/40 μA (high filter). This mode is capable of detecting more than 20 elements in particulate geosolids (from K to Bi) but here we focus on trace metals that were readily detected in a preliminary study of estuarine sediments (As, Cr, Cu, Pb, Sb, Sn, Zn; Turner et al., 2017) as well as metals that act as potential geochemical proxies or indicators of analytical performance (Ca, Fe, K, Rb).

In the laboratory, the instrument was configured nose-upwards in a 4000 cm^3 accessory stand and activated remotely through a laptop and at an operator distance of 2 m. In the field, the instrument was configured nose-upwards in a 300 cm^3 portable test stand (described in detail elsewhere; Turner, 2017) and activated and operated likewise. Spectra arising from sample counting were quantified by fundamental parameter coefficients to yield metal concentrations in $\mu g\ g^{-1}$ and with a measurement counting error of 2σ (95% confidence) that were downloaded to the laptop via Niton data transfer (NDT) software.

2.2. Sampling and sample characteristics

Estuarine sediment samples were collected from the Tamar and its tidal tributary, the Tavy. The watershed of the Tavy and the upper catchment of the Tamar are dominated by moorland, managed forest and agricultural land but remain highly contaminated by various trace metals (and mainly As and Cu) from historical mining activities, while the lower catchment of the Tamar is partly urbanised and supports various facilities for the maintenance and repair of boats and ships. Fine, surficial (depth < 5 mm) intertidal muds and silts were targeted at the locations shown in Figure 1 and during 2017 and early 2018 in order obtain a variety of relatively homogeneous materials that required minimal processing. Specifically, (i) a number of samples were collected from the Tamar and Tavy as and when required in order to undertake various tests in the laboratory, (ii) a field transect was undertaken along the axis of the Tamar at nine sites from above its tidal limit to about 5 km from the mouth (including locations known to be impacted by metal inputs from adits and streams), and (iii) a ~ 20 m cross section of the intertidal zone was conducted on site in the Tavy estuary at a location bordered by saltmarsh; here, sampling was undertaken at 3 m intervals (measured using a 30 m tape measure) and included a number of anoxic, subsurface sediments that were accessed from pits dug into the substrate.

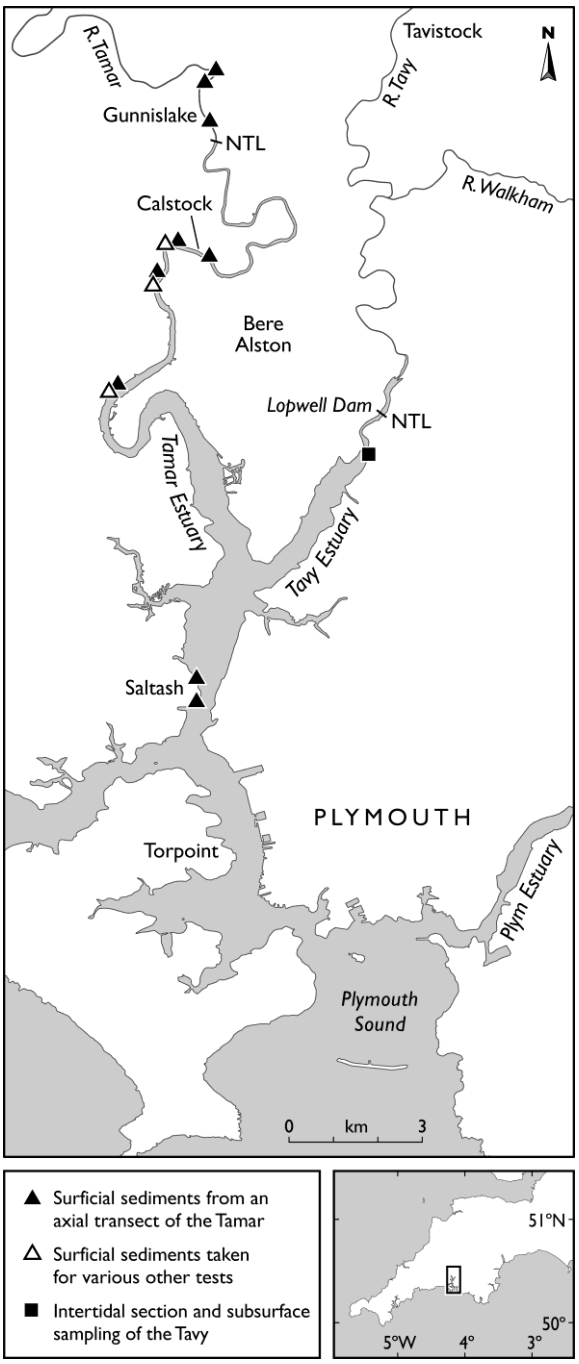

141

142 **Figure 1: Sampling locations in the Tamar and Tavy estuaries, southwest England.**

143 **NTL = normal tidal limit.**

144

145 About 50 to 100 g of material were collected with a plastic trowel and transferred directly

146 into a clear, minigrip, re-sealable polyethylene bag (1.25 g, 12 cm x 9 cm below the seal;

147 Polybags Ltd, Greenford UK) for direct measurement in the field or for return to the

148 laboratory and subsequent testing. Bags were selected on the basis of rigidity and strength,

thickness 50 μm per face), water-tightness, sample accessibility and material purity. Regarding the latter, analysis by the Niton XL3t in a low density 'plastics' mode and with thickness correction revealed no metallic contamination of clear polyethylene but the presence of small quantities of Ti and Ba in the white labelling panel. Once bagged, samples were squeezed gently in order to detect any larger extraneous particles, like shell fragments, grit and plant debris. Occasional particles were eliminated with tweezers, with sieving through a 1 mm plastic mesh and into a polyethylene bowl required in cases where larger solids were more abundant.

Particle size analysis was performed on aliquots of selected samples using a Malvern Instruments Mastersizer 2000 equipped with a He-Ne laser. Briefly, subsamples were introduced to a Hydro-G sample unit holding a 1 L solution of 0.1% sodium hexametaphosphate in Elga ultrapure water (UPW). The contents were continuously stirred to ensure proper resuspension and subsequently ultrasonically dispersed before successive 30-s measurements (n = 5) were performed in the diffraction cell. Results revealed volume weighted means in the range 50 to 150 μm, and 5^{th} and 95^{th} percentile values of about 5 μm and between about 200 to 700 μm, respectively.

2.3. Sediment testing by XRF in the laboratory

The effects of interstitial water on XRF measurements through both contribution to sample mass and x-ray attenuation were examined on two samples of different metallic composition from the Tamar estuary. After weighing on a Sartorius two-figure balance, bagged samples were placed sideways and with the labelling panel facing upwards over the detector window, ensuring that the depth of material was at least 8 mm (an assumed critical thickness of a sediment-water mixture; Parsons et al., 2013). With the accessory stand shield closed, samples were counted six times at the same (50 mm^2) location in order to determine

175 measurement precision and a further six times at different locations in order to evaluate
176 spatial heterogeneity.
177
178 Samples were subsequently freeze-dried in an Edwards Super Modulyo for 96 h before being
179 reweighed, homogenised (by gently shaking and manually kneading the bagged contents),
180 and reanalysed six times at one location and six times at multiple locations. Increasing
181 quantities of UPW were then added in order to wet samples with the contents in their
182 original bags reweighed and reanalysed by XRF as above after each aqueous addition. Here,
183 water was dispensed using a Jencons Sealpette 1 ml micropipette and dispersion of water
184 throughout the sample was accomplished by careful manual manipulation of the bagged
185 contents and subsequent lateral shaking at 500 rpm for up to 30 minutes on an Ika KS 130
186 shaker. Based on preliminary investigations into the moisture content of intertidal mud and
187 practical constraints that included the ability to wet sediments homogenously, the fraction of
188 added UPW to total mass was varied between about 0.2 and 0.7.
189
190 Any effects on XRF measurements arising from particle size and mineralogical variations
191 within and between samples were evaluated by analysing a number of dried sediments from
192 the Tamar and Tavy estuaries (n = 12) in re-sealable bags both before and after milling (to <
193 50 μm). The latter was accomplished in a series of 80 mL agate bowls, each containing five
194 20 mm agate milling balls, using a Fritsch planetary mill (model Pulverisette 5) at 300 rpm
195 for 3 min. Primary and secondary x-ray attenuation by the re-sealable bags was tested on a
196 number of reference materials (NIST 2709, Agricultural Soil; MSH101, loam; GBW07318,
197 stream sediment) and milled, freeze-dried Tamar sediments that had been packed into
198 individual, polyethylene XRF sample cups (Chemplex series 1400, 21-mm internal
199 diameter) and collar-sealed with 3.6 μm SpectraCertified Mylar polyester film. Here,

200 samples were analysed six times directly through the polyester film and then six times
201 through an additional 50 μm layer of polyethylene cut from the face of a bag.
202
203 Dried and milled materials prepared in customised sample cups eliminate the absorptive and
204 matrix effects of moisture and polyethylene and minimise variations in particle size or
205 texture. XRF results obtained through direct the analysis of samples processed this way
206 therefore afford optimal measures of absolute, dry weight concentrations, while reference
207 materials processed and analysed similarly serve as a measure of the accuracy of the
208 technique. To this end, mean measured metal concentrations and certified concentrations for
209 three reference geosolids, compared in Table 1 on a dry weight basis ([Me-dw], μg g^{-1} dw),
210 reveal agreement that is always better than 25% apart from Cr and K in NIST 2079
211 (agreement within 30%), and repeatability that is better than 10% in most cases.
212
213 **Table 1: Certified and measured concentrations of metals ([Me-dw], μg g^{-1} dw) in three**
214 **reference materials. Errors represent 95% confidence intervals arising from six**
215 **measurements (measured) or an unspecified number of measurements (certified) and <**
216 **LOD denotes a mean concentration below the limit of detection.**

reference material	metal	certified, μg g^{-1} dw	measured, μg g^{-1} dw
NIST 2709	As	10.5 ± 0.3	9.6 ± 1.2
	Ca	19,100 ± 900	17,800 ± 318
	Cr	130 ± 9	92.6 ± 10.8
	Cu	33.9 ± 0.5	28.1 ± 5.2
	Fe	33,600 ± 700	34,000 ± 157
	K	21,100 ± 600	15,600 ± 179
	Pb	17.3 ± 0.1	15.2 ± 2.2
	Rb	99.0 ± 3	91.3 ± 2.1
	Zn	103 ± 4	101 ± 5.4
MSH101	As	1090 ± 16.7	1220 ± 11.3
	Zn	1100 ± 16.8	1260 ± 15.8
GBW07318	As	18 ± 2	22.2 + 5.5
	Cr	243 ± 16	198 ± 8.5
	Cu	66 ± 6	60.3 ± 7.8
	Pb	66 ± 7	58.5 ± 5.7
	Rb	87 ± 7	83.4 ± 0.9
	Sn	9.5 ± 1.7	<LOD
	Zn	165 ± 15	174 ± 4.0
	Ca	25,000 ± 710	20,600 ± 325
	K	19,200 ± 830	16,800 ± 194

217

218

219

220 **3. Results and Discussion**

221 *3.1. Measures of LOD, precision and heterogeneity for sediment in the fresh and dried states*

222 Measurement limits of detection (LOD) and measures of precision and heterogeneity for the
223 different metals arising from multiple analyses (n = 6) of three bagged Tamar estuary
224 samples are presented in Table 2. LODs are given both on a fresh weight basis ([Me-fw], μg
225 g^{-1} fw), as would be tested in the field, and on a dry weight basis ([Me-dw], μg g^{-1} dw) after
226 freeze-drying in the laboratory. LOD is based on the counting error and defined as 3σ, and is
227 either reported directly by the instrument where an element is undetected or is derived from
228 multiplication of 2σ by 1.5 when detection is achieved. For a given counting time and
229 sample thickness (above a critical depth), LODs are specific to the precise composition of
230 the sample (and, in particular, the relative abundance of metals whose fluorescent x-ray

231 energies are similar) and limits reported in the Table, based on the lowest mean values
232 among the three samples tested, should be regarded as approximate. Thus, in the dry state,
233 LODs range from < 20 μg g^{-1} for As, Cd, Pb and Rb to > 100 μg g^{-1} for Ca, Co, Fe and K,
234 while in the fresh state LODs are always lower than corresponding values after freeze-drying
235 and range from < 10 μg g^{-1} for As, Cd, Pb and Rb to > 100 μg g^{-1} for Ca, Fe and K. Lower
236 LODs in the fresh state may be related to the ability to place a wet paste or slurry closer to
237 and flatter against the detector window than a dried, particulate material (Turner et al.,
238 2017), but once concentrations in fresh samples had been normalised to a dry weight basis
239 ([Me-dw*], μg g^{-1} dw*) by correcting for the fraction of water present, f_w:
240
241 $$[\text{Me-dw*}] = [\text{Me-fw}]/(1-f_w) \qquad (1)$$
242
243 LODs were, in general, considerably greater than corresponding limits when analysed dry.
244 Within these constraints, As, Ca, Cu, Fe, K, Pb, Rb, Sn and Zn were detected in all cases and
245 in both the fresh and dry states and Cr was detected in most cases when fresh and in all cases
246 when dry.
247
248 **Table 2: Limits of detection (LOD) and measures of precision and spatial heterogeneity**
249 **for metals in three Tamar estuary sediments analysed six times in resealable bags in**
250 **the fresh state and after freeze-drying. LOD refers to the lowest mean value while**
251 **precision and heterogeneity are reported as a range of values (with the exception of Cr**
252 **in the fresh state; *n* = 1 or 2).**

	fresh			dry		
metal	LOD, μg g^{-1} fw	precision, %	heterogeneity, %	LOD, μg g^{-1} dw	precision, %	heterogeneity, %
As	6.8	1.5-9.6	8.2-19.0	15.6	1.0-4.8	5.4-12.6
Ca	189	2.9-4.7	7.5-22.3	618	2.6-2.7	6.1-10.2
Cr	33.9	9.6	9.6; 13.0	47.2	14.9-18.4	18.3-38.1
Cu	14.9	2.2-16.7	8.9-13.0	29.6	1.3-3.6	4.2-7.7
Fe	197	0.6-1.0	2.0-8.0	515	0.3-0.6	3.0-8.5
K	210	2.4-3.7	5.6-15.1	697	1.3-1.5	3.2-5.5
Pb	6.5	2.0-5.0	3.2-13.4	14.7	1.7-2.1	2.7-5.9
Rb	3.0	1.4-2.5	4.0-11.2	7.7	0.7-2.1	1.5-2.9
Sn	14.1	6.5-25.4	16.2-26.3	27.8	4.0-12.4	11.0-18.7
Zn	12.1	2.8-4.4	1.7-12.3	27.0	2.0-2.6	2.9-8.1

Precision is shown in Table 1 as the relative standard deviation (rsd, %) resulting from repeated measurements of the same 50 mm^2 area of a bagged sample and for a given metal is presented as the minimum and maximum value arising from the three samples tested. When analysed fresh, precision ranges from < 1% for Fe in all three samples to > 15% for Cu and Sn in one case each. In the dry state, the minimum and maximum precisions are always better (or rsds always lower) than corresponding values in the fresh state, despite greater analytical sensitivity achieved for the latter.

Heterogeneity, defined as the rsd of multiple measurements performed at different 50 mm^2 locations of the same sample, is also presented in Table 1 in terms of minimum and maximum values. In nearly all cases, spatial heterogeneity is greater than corresponding precision, with differences in some cases about an order of magnitude. Heterogeneity may be attributed to the variation of a number of parameters across a given sample contained within a re-sealable bag that include material thickness, water content and dispersion, grain size and porosity and sediment settlement (see below), as well as any inherent variations in the distributions of trace or geochemical metals themselves. Without further material processing, heterogeneity is considered a better indicator of variation than precision and is, therefore, adopted as a default measure in all further testing.

3.2. Effects of sample milling on metal concentrations returned by XRF

In order to explore the sources of analyte spatial variation further, a greater variety of samples collected from the region on a number of occasions (n = 12) was analysed as above and at different locations with respect to the face of the re-sealable bag after freeze-drying and then after milling to a finer and more homogenous powder. Although we observed greater variability within the same sample before milling, mean concentrations showed good agreement with corresponding mean concentrations after homogenisation. Thus, regression coefficients defining the association of the two measures exceeded 0.9 for all metals considered with the exception of Cr and Fe (where the range in concentrations tested was relatively small), with slopes that were within 10% of unit value in all cases with the exception of Pb (Table 3). These observations suggest that spatial variation in metal concentrations is at least partly associated with an inherent variation within samples when dried (including variations in grain size and mineralogy) but that averaging of multiple analyses without milling generally gives a good measure of overall concentration. In the fresh state, we surmise that greater variation arises from the presence and heterogeneous dispersion of water within the sample, whose effects on XRF measurements are examined in more detail below.

Table 3: Slopes and regression coefficients defining the relationships between mean metal concentrations ([Me-dw], μg g^{-1} dw; n = 6) measured on 12 dried samples before and after milling.

metal	Slope	r^2
As	1.017	0.980
Ca	0.904	0.992
Cr	0.909	0.238
Cu	0.994	0.944
Fe	1.009	0.747
K	1.003	0.998
Pb	0.859	0.999
Rb	1.038	0.950
Sn	0.966	0.968
Zn	0.978	0.980

295

296

297 *3.3. Effects of water on metal concentrations returned by XRF*

298 With the effects of moisture on LOD and measurement variation established, the effects of
299 interstitial water on metal concentrations returned by the XRF were investigated more
300 systematically. Figure 2 shows the results of XRF analyses performed on two Tamar estuary
301 samples, originally in the dry state, over a range of f_w values that were engendered by
302 incremental additions of UPW. Metal concentrations are shown on a dry weight basis as
303 determined directly after freeze-drying ([Me-dw], μg g^{-1} dw) or on a dry weight basis but as
304 determined in the wetted state and after correction for the mass of water present ([Me-dw*],
305 μg g^{-1} dw*; equation 1). Where errors were relatively high or variable (e.g. Sn in both
306 samples and As, Cr and Fe in one sample), there were no clear differences in mean metal
307 concentrations over the range of water content tested. However, in the majority of cases
308 there was a reduction in mean concentration with increasing water content over all or part of
309 the range tested that was often significant according to one-way ANOVA and a post-hoc
310 Tukey test ($\alpha = 0.05$). Specifically, there was generally a minimum in dry weight elemental
311 concentration at an f_w of about 0.5 or 0.6 and a subsequent increase in concentration with
312 further additions of UPW. This type of distribution can be understood from the interplay of
313 two competing effects: namely, the attenuation of x-rays by the interstitial medium and the
314 settlement of sediment in a slurry-type preparation.

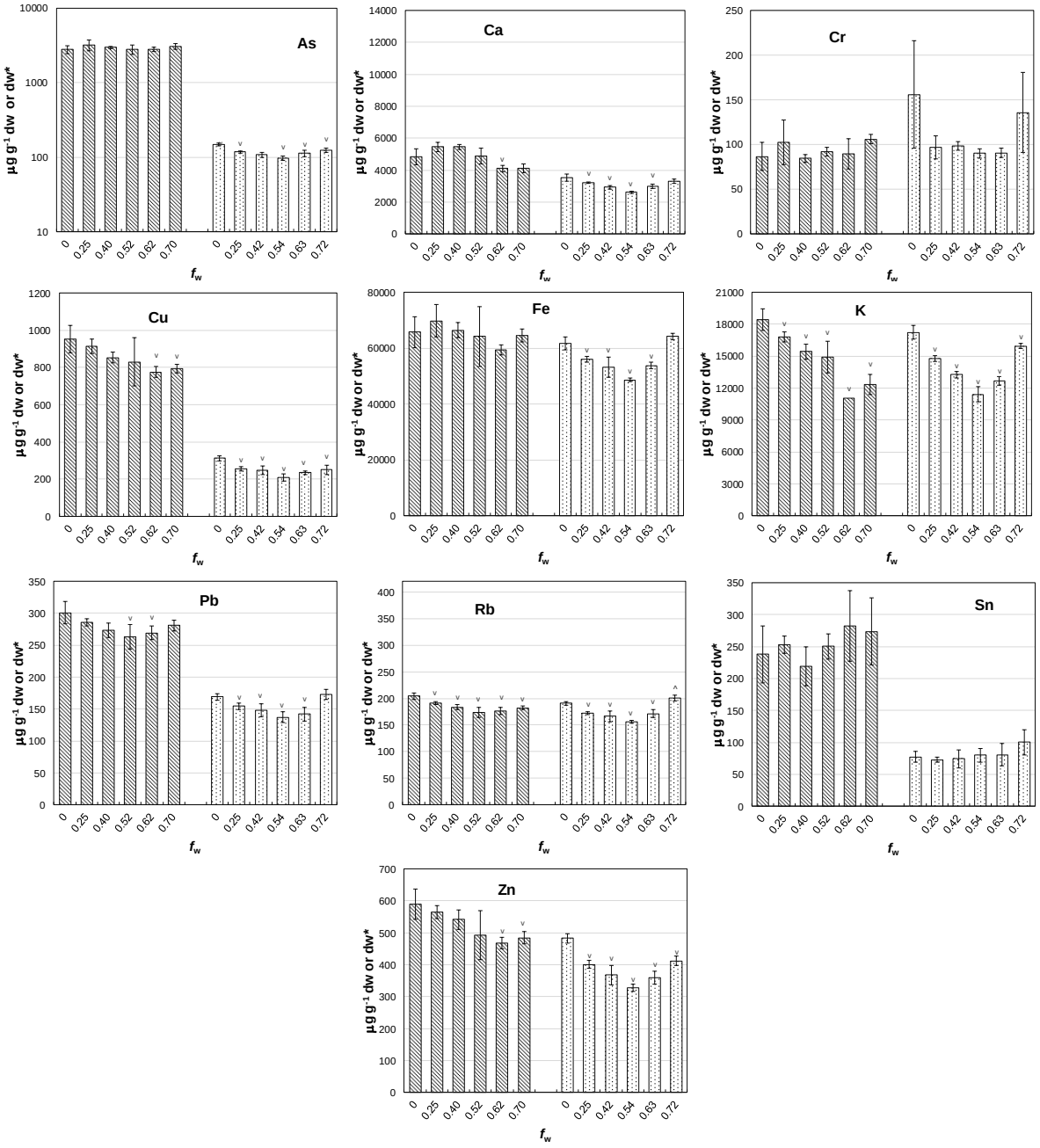

Figure 2: Dry weight metal concentrations in two Tamar estuary sediment samples (shaded differently) that were analysed in the dry state ([Me-dw], µg g^{-1} dw; f_w = 0 only) and subsequently in the fresh state after incremental additions of UPW ([Me-dw*], µg g^{-1} dw*; equation 1). Errors represent one standard deviation about the mean of six measurements undertaken at different sample locations and v or ^ indicate mean concentrations that are significantly lower or higher than corresponding mean concentrations reported for the dry state (one-way ANOVA, α = 0.05).

Because x-rays are attenuated (through photoelectric absorption and scattering) to a considerably greater extent by liquid water than by air, the presence of interstitial water reduces the energy available for sample excitation and decreases the sensitivity of the analysis, at least when converted to a dry weight basis (Ge et al., 2005). Attenuation of this nature will affect metals differently in terms of analytical sensitivity and measurement error depending on the primary x-ray energies required for excitation (i.e. low, main or high filters; see above) but its overall impact should be directly related to the percentage of water present. The water-attenuation of fluorescent x-rays that are registered by the detector results in lower counts and apparent concentrations, an effect whose magnitude is predicted to be metal-specific (and dependent on the energies of the principal lines used in detection) and directly related to the quantity of water present.

The results in Figure 2 are partly consistent with secondary x-ray attenuation in that reductions in [Me-dw*] with increasing f_w are most pronounced for K, whose K_{a1} line energy is the lowest among the elements considered (3.31 keV), and not evident for Sn, whose K_{a1} energy line is the highest (25.27 keV). However, the effects of x-ray attenuation also appear to be offset to differing extents above a fractional water content of about 0.5 to 0.6. Here, we attribute an increase in apparent concentration to the settlement of material from slurries of a relatively high water content during the analysis. Partial separation of solid and aqueous media results in analytes that are closer to the detector window and a reduced thickness of water for primary and secondary x-ray attenuation compared with samples where sediment is in a more homogenous suspension. Overall, therefore, analysis of fine sediment samples in the fresh state appears to be limited to f_w values of about 0.5 to 0.6 before the effects of settlement become evident, with dry weight-normalised results that are within 20% of results when analysed dry with the exception of K.

3.4. Attenuation of fluorescent x-rays by polyethylene

Because sediment samples are contained in polyethylene bags, it was necessary to evaluate the potential impacts on metal measurements arising from x-ray attenuation by polyethylene. Here, various milled samples (n = 6; including three reference sediments and soils) contained in XRF cups were analysed at different locations through the ~ 4 μm polyester retaining film both with and without a 50 μm layer of polyethylene derived from a resealable bag placed above the detector window. Polyethylene has a similar mass attenuation coefficient to water across the energy range of 0 to 50 keV (Hubbell and Seltzer, 1996) but its thickness in the current context is considerably more uniform both within and between samples. Table 4 compares results for each element considered in terms of the slope and linear regression coefficient arising from mean concentrations ([Me-dw], μg g^{-1} dw) in the presence and the absence of polyethylene. In all cases, regressions were highly significant (p < 0.01) and coefficients exceeded 0.93, with slopes in only three cases deviating from unit value by more than 5%; specifically, those for Ca, Cr and K were about 0.80, 0.86 and 0.74, respectively (equivalent to attenuations of about 20%, 14% and 26%, respectively), reflecting the relatively low energies of their respective K lines (K_{a1} = 3.69 keV, 5.41 keV and 3.31 keV).

Table 4: Slopes and regression coefficients defining the relationships between mean metal concentrations ([Me-dw], μg g^{-1} dw; n = 6) measured on six dried soil and sediment samples (including three reference materials) in the presence and absence of a 50 μm layer of polyethylene.

metal	slope	r^2
As	0.969	1.000
Ca	0.798	0.998
Cr	0.863	0.937
Cu	0.972	0.998
Fe	0.957	0.993
K	0.735	0.984
Pb	0.958	1.000
Rb	0.954	0.996
Sn	0.956	1.000
Zn	0.988	1.000

375

376 *3.5. Combined effects of water and polyethylene*

377 The results of the present tests performed on fine estuarine sediments are qualitatively
378 consistent with results obtained for floodplain soils by Parsons et al. (2013). That is, a
379 reduction in apparent concentration is observed with increasing interstitial water content and
380 in the presence of a polyethylene barrier, effects that are most pronounced for lighter
381 elements with relatively low energy x-ray emission lines like Ca and K. Quantitatively,
382 however, the impacts of attenuation by water and polyethylene on sediment appear to be
383 lower than those observed for soils and agreement between measurements performed on
384 fresh and dried sediments is within 20% up to a fractional water content of about 0.6 for
385 elements whose atomic mass is greater than Ca.

386

387 As means of a summary thus far, Table 5 compares portable XRF results obtained from
388 multiple analyses of a Tamar estuary sample that had undergone each step of processing
389 described above. Specifically, concentrations of metals are shown when sediment was
390 analysed (i) bagged and in the fresh state, and after normalisation for interstitial water
391 content according to equation 1, (ii) bagged and after freeze-drying, (iii) bagged and after
392 milling, and (iv) packed into a sample cup after milling. In general, results become
393 progressively more precise through each stage and as the optimal measure of absolute
394 concentration is approached. Significantly, however, results obtained when the sample was
395 analysed fresh and bagged and corrected for moisture are statistically indistinguishable from

optimal results (according to a series of paired *t*-tests; $\alpha = 0.05$) for all metals with the exception of Cu, Ca and K; here, concentrations were about 15%, 35% and 45% lower when analysed fresh, with the relatively large discrepancies for the latter metals reflecting the combined effects of secondary x-ray attenuation by both water and polyethylene described above.

Table 5: A comparison of metal concentrations in a sample of Tamar sediment that had been analysed fresh and normalised for moisture content (equation 1), analysed dry, analysed after milling and analysed after milling and packing in an XRF sample cup. Errors represent one standard deviation about the mean of 6 or 7 analyses performed at different locations with respect to the sample bag or polyester surface.

	fresh	dry	dry-milled	dry-milled-packed
metal	$\mu g\ g^{-1}$ dw*	$\mu g\ g^{-1}$ dw	$\mu g\ g^{-1}$ dw	$\mu g\ g^{-1}$ dw
As	116±6.7	128±4.8	128±3.1	130±5.7
Ca	3800±321	4200±112	4430±122	5600±60.6
Cr	107±10	102±21.8	90.8±10.5	114±17.6
Cu	234±23	284±14.9	264±12.2	273±11.6
Fe	52,900±2220	53,300±889	50,900±597	54,300±326
K	11,300±659	16,200±713	15,000±289	20,700±314
Pb	147±4.7	151±4.7	149±2.6	154±2.4
Rb	166±4.2	170±4.8	165±2.7	169±2.0
Sn	84.3±22.8	82.2±11.7	86.4±10.0	89.0±6.0
Zn	386±34.5	427±11.7	407±10.2	429±12.6

3.6. XRF analysis on site

Within the constraints and variations associated with the analysis of fresh sediments, the XRF spectrometer was tested on site during two field surveys. Thus, firstly, an axial transect of the Tamar estuary was undertaken from above its tidal limit to about 5 km from its mouth and at the nine locations shown in Figure 1. Here, the instrument, portable test stand and laptop were driven to the foreshore where they were configured directly, or with the use of the equipment carry cases, on a flat, firm surface. Surficial samples were collected with a

plastic trowel, manually checked for extraneous material, and analysed directly and at six 50 mm^2 locations in resealable polyethylene bags under the operating conditions defined above. Provided that samples were readily accessible, the time required at each site was less than 20 minutes for two trained operators working simultaneously.

Secondly, a transect of the intertidal zone on the Tavy estuary at the location shown in Figure 1 was undertaken from the saltmarsh to near the low water mark; this survey also included sampling below the sediment surface from pits dug using a garden spade. As above, the equipment was set up on the foreshore and each sample was analysed directly and at six locations. Here, once the equipment had been set up on site, a throughput of about six to eight samples per hour was readily accomplished by two operators, with a range of measurements, in theory, limited by the life of the laptop and XRF batteries (about two and four hours, respectively). On return to the laboratory, samples from both surveys were weighed, freeze-dried, re-weighed and re-analysed in the laboratory accessory stand.

The results of the axial and inter-tidal surveys are summarised in Figure 4 in terms of concentrations determined on site and after correction for water content, ([Me-dw*], $\mu g\ g^{-1}$ dw*; equation 1), versus concentrations determined in the laboratory and after freeze-drying, ([Me-dw], $\mu g\ g^{-1}$ dw). Here, linear regression analysis has been performed on all metals combined since the range of concentrations encountered for many individual elements was too small to determine any degree of association. Thus, overall, the slopes of the best-fit lines were within 15% of unit value and regression coefficients exceeded 0.95 for both surveys, with better fits that were closer to unit value resulting when data for Ca and K were excluded from the analysis. The mean and one standard deviation of f_w for the axial and intertidal transects were 0.555 ± 0.09. and 0.559 ± 0.123, respectively, suggesting that a value of close to 0.5 affords a good approximation of this parameter, at least in the current

environments, when gravimetric analysis is not possible or an immediate assessment of sediment geochemistry or contamination is required.

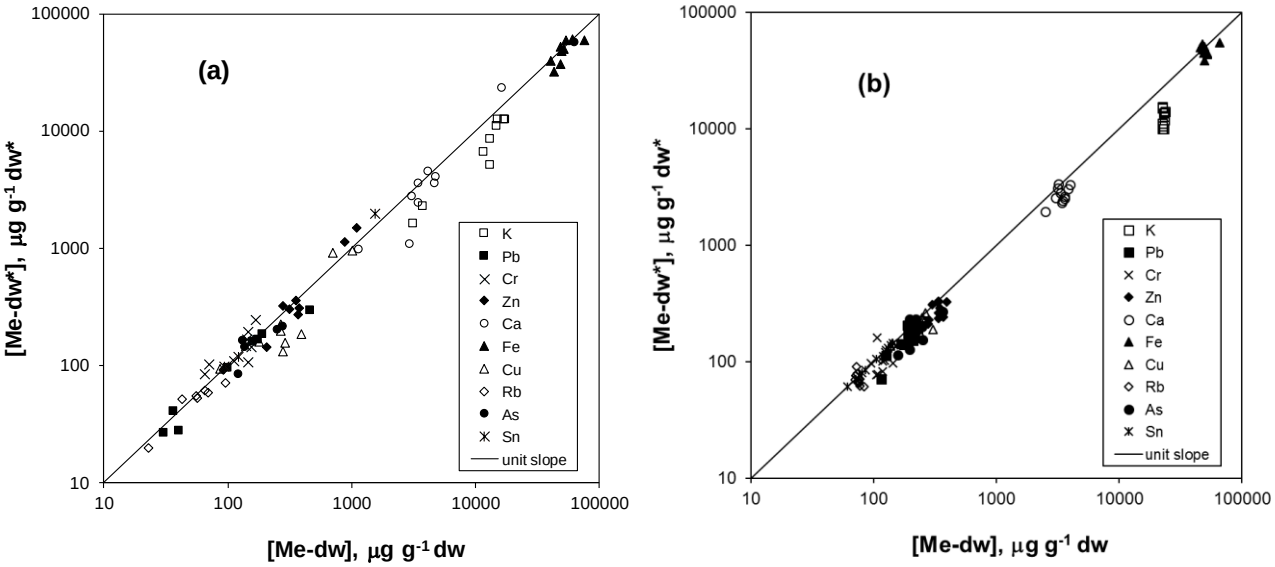

Figure 4: Mean concentrations of metals measured on site and subsequently corrected for fractional water content according to equation 1 ([Me-dw*], µg g^{-1} dw*; *n* = 6) versus corresponding mean concentrations measured after freeze-drying ([Me-dw], µg g^{-1} dw; *n* = 6) in the (a) Tamar estuary and (b) Tavy estuary. Errors are not shown for clarity and the solid line represents unit slope. Results of linear regression analysis were as follows: (a) $y = 0.916x$, $r^2 = 0.974$, $p < 0.001$; (b) $y = 0.870x$, $r^2 = 0.954$, $p < 0.001$; and after exclusion of Ca and K data were: (a) $y = 0.923x$, $r^2 = 0.982$, $p < 0.001$; (b) $y = 0.930x$, $r^2 = 0.985$, $p < 0.001$.

3.7. Rb as a proxy for grain size and water content

Employing XRF to determine metal concentrations in marine sediment cores, Tjallingii et al. (2007) suggest using Cl as a proxy for sea water content when sections are analysed in the wet state. However, the XL3t series of Niton analysers are not calibrated for Cl in modes designed for particulate geosolids. Moreover, should the Cl intensity be quantified, estuaries are characterised by such strong spatial and temporal variations in salinity that measurement

of the latter in the interstitial environment would also be required. Accordingly, an indirect means of estimating the interstitial water content on site was explored based on the premise that it bears some relationship with sediment porosity, hence grain size.

Aluminium is often employed as a sediment grain size normaliser (Nolting et al., 1999; Din, 1992) but is too light to be analysed by conventional portable XRF unless measurements are performed in a helium atmosphere. Iron has also been employed to compensate for grain size variations (Loring, 1991) but in the current setting this metal has a strong anthropogenic signal from historical mining activities (Mighanetara et al., 2009). An alternative normaliser that has been used in some studies is Rb, whose concentration in sediment bears an inverse relationship with grain size through substitution for K in fine-grained clays and whose distribution is unaffected by anthropogenic inputs (Rae, 1995; Turner and Lewis, 2018). With respect to portable XRF, Rb has the additional advantages of being easy to detect and relatively little affected by water or polyethylene attenuation.

In Figure 5, the concentration of Rb determined in sediment in the fresh state ([Rb-fw], $\mu g\ g^{-1}$ fw) during the axial transect of the Tamar and the inter-tidal transect of the Tavy is plotted against 1 - f_w determined subsequently by gravimetry. For the inter-tidal transect, where material is likely similar in geology and origin across the relatively small area surveyed, the goodness of fit is excellent; for the axial transect, encompassing a wider range of lithological materials and sources, the data are more scattered but the fit is still significant. This relationship is not predicted from simple porosity considerations alone where an increase in grain size of a given shape is accompanied by decreasing void space for the occupation by interstitial water (Roychoudhury, 2001). Here, however, all samples were rather fine and partially drained, with particle size measurements revealing a relatively small range in median particle diameter and surface area. Across such a small size range, additional,

494 confounding effects may be more significant among the samples that contribute to water
495 retention, such as variations in grain density, size distribution, organic matter content, degree
496 of consolidation and time-age of deposition.
497
498 Regardless of the precise causes of the relationships observed, measurement of Rb appears to
499 provide a suitable, direct means of estimating interstitial water content provided that an
500 empirical calibration between [Rb-fw] and 1 - f_w (with a slope, *b*, and intercept, *a*) is
501 established for the environment of interest. In practice, therefore, the water-corrected metal
502 concentration on a dry weight basis, [Me-dw*], may be calculated from the metal
503 concentration determined on a fresh weight basis and in the field, [Me-fw], as follows:

504 $$[\text{Me-dw*}] = \frac{[\text{Me-fw}]}{([\text{Rb-fw}] - a)/b} \qquad (2)$$

505
506

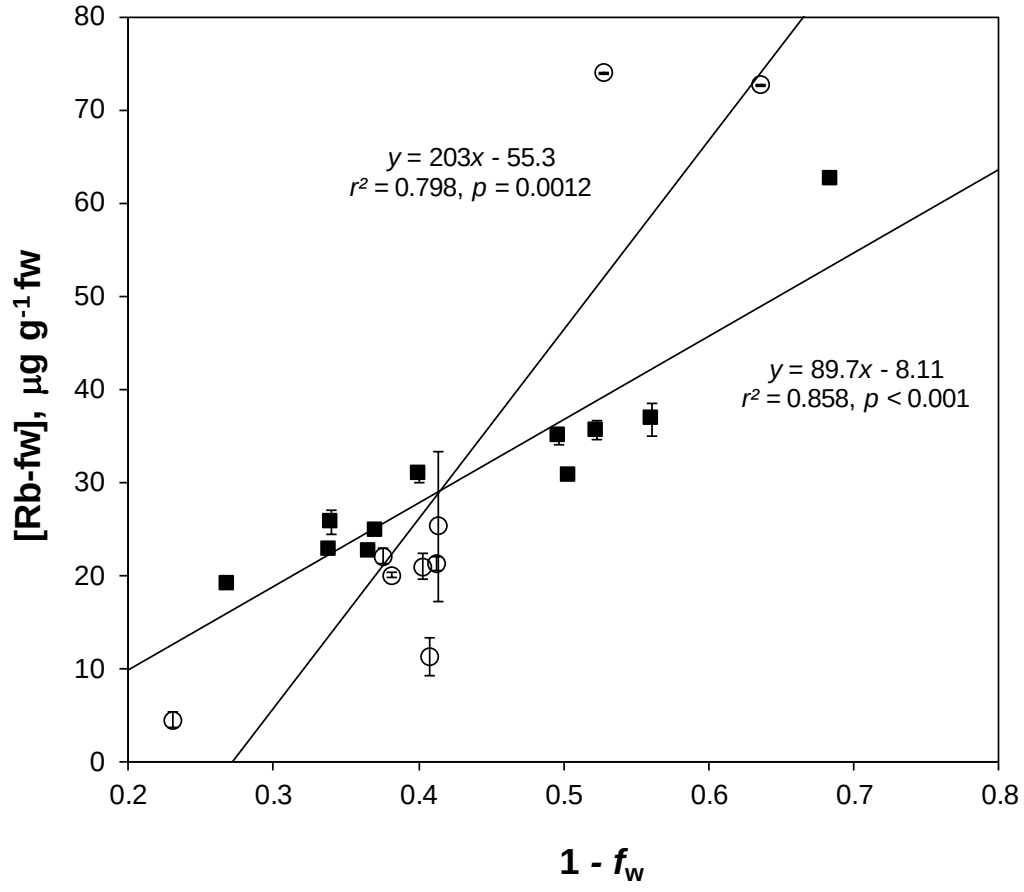

507

Figure 5: Concentration of Rb determined on site and on a fresh weight basis ([Rb-fw], μg g^{-1} fw) versus 1 - f_w for sediments from the axial transect of the Tamar (o) and the inter-tidal transect of the Tavy (■). Errors represent the standard deviation about the mean of six measurements and annotated are best-fit regression lines and results of linear regression analysis.

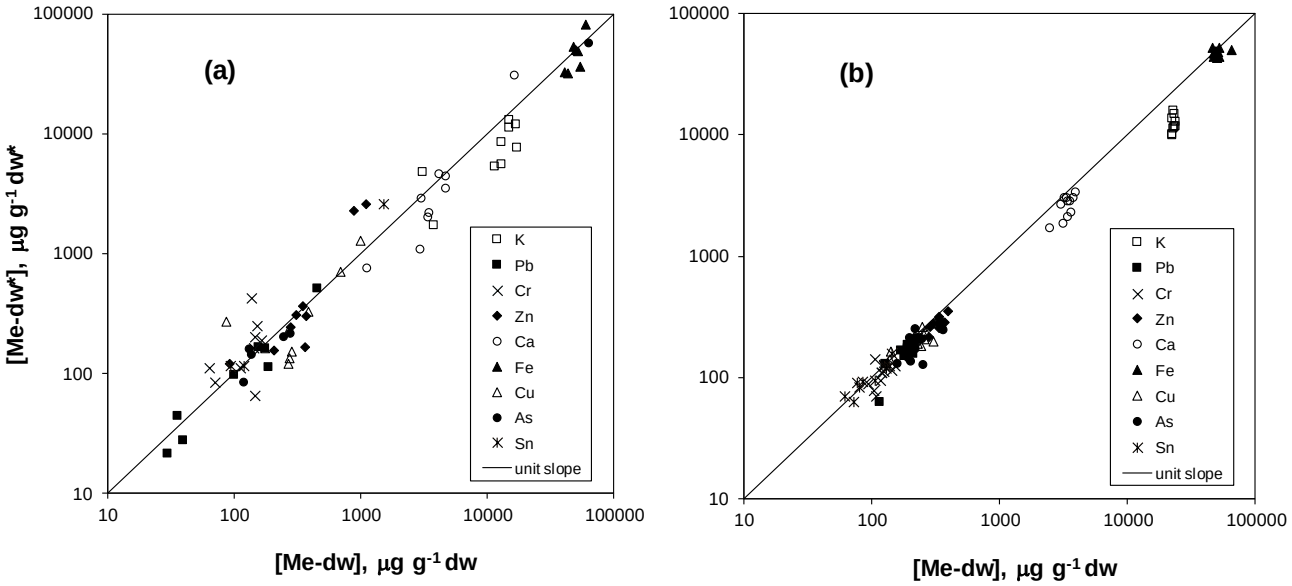

Figure 6: Mean concentrations of metals measured on site and subsequently corrected empirically according to equation 2 ([Me-dw*], μg g^{-1} dw*) versus corresponding mean concentrations measured after freeze-drying ([Me-dw], μg g^{-1} dw) in the (a) Tamar estuary and (b) Tavy estuary. Errors are not shown for clarity and the solid line represents unit slope. Results of linear regression analysis were as follows: (a) $y = 1.085x$, $r^2 = 0.925$, $p < 0.001$; (b) $y = 0.862x$, $r^2 = 0.954$, $p < 0.001$; and after exclusion of Ca and K data were: (a) $y = 1.102x$, $r^2 = 0.940$, $p < 0.001$; (b) $y = 0.923x$, $r^2 = 0.987$, $p < 0.001$.

Direct, fresh weight measurements taken along the axis of the Tamar estuary and the transect of the Tavy estuary were empirically corrected according to equation 2 and using the coefficients defined in Figure 5 (a = -55.3 and b = 203, and a = -8.11 and b = 89.7,

respectively) and are plotted against measurements made after freeze-drying in Figure 6. Slopes of the best-fit lines defining all data points were within 15% of unit value and regression coefficients exceeded 0.9 for both surveys and, as above, better fits and slopes that were closer to unit value resulted when data for Ca and K had been excluded.

Results derived from this empirical approach are exemplified for specific elements in Figure 7. Thus, here, concentrations of Cu in surficial sediments are plotted as a function of distance along the axis of the Tamar estuary and concentrations of As in surficial and anoxic (~ 5 cm depth) sediments are shown as a function of distance across the mudflats of the Tavy estuary. In the Tamar, distributions of Cu are consistent with two the principal sources of the metal: inputs from a dense array of historical mine workings above the tidal limit (Mighanetara et al., 2008), and a more diffuse input from boating activities (e.g. antifouling paint) towards the mouth of the estuary (Turner, 2010). In the Tavy, distributions of As at the surface are rather uniform, reflecting the homogenous dispersion of fine-grained material throughout the intertidal zone; however, concentrations are significantly lower at depth (according to a series of paired *t*-tests; $\alpha = 0.05$) because of the dissolution of hydrous Fe oxide host phases under reducing conditions (Chaillou et al., 2003).

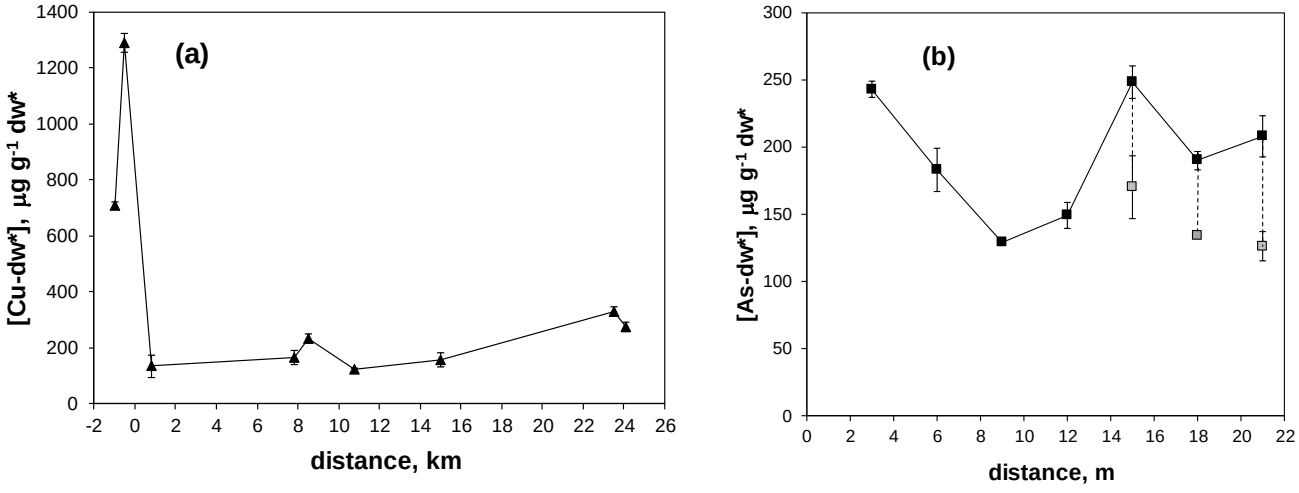

Figure 7: Mean metal concentrations measured on site and subsequently corrected empirically according to equation 2 ([Me-dw*], μg g^{-1} dw*). (a) Cu in surficial sediments of the Tamar estuary as a function of axial distance from the tidal weir and (b) As in surficial sediments (filled squares) and anoxic sediments (shaded squares) as a function of distance from the high water mark. Errors represent the standard deviation about the mean of six measurements.

3.7. Concluding remarks

The present study has shown that on site XRF analysis (using a Niton XL3t instrument) returns concentrations of metals in fine (milled), dried, particulate geosolids in a standardless mining mode with good accuracy over a range of concentrations typical of estuarine sediments. When samples are analysed fresh, however, the presence of water reduces signal intensity through both the dilution of material and the attenuation of exciting and fluorescent x-rays. While these effects can be corrected for empirically up to moisture contents of about 60%, they impose constraints on the ability to determine dry-weight concentrations of metals directly in the field, with approximate values restricted to elements heavier than Cr and gained by assuming a generic fractional water content. A more practical means of determining the relative degree of metal contamination within or between estuaries, including axial distributions and localised transects, was to correct fresh-weight concentrations determined in the field with respect to Rb, an element that was simultaneously able to correct for both variations in granulometry and interstitial water content. This approach has the potential to detect subtle changes in trace metal contamination over small areas as well as more significant hot-spots of metals arising from localised sources. In the field, direct and immediate results may be used to guide a research

strategy, assist with rapid decision-making or target samples for further characterisation in the laboratory.

Acknowledgements

This study was partly funded by a HEIF Plymouth University Marine Institute grant. Drs Gillian Glegg and Charlotte Braungardt (PU) are thanked for assistance with sample collection.

References

Al-Jundi, J., 2001. Instrumental neutron activation analysis (INAA) of estuarine sediments. Journal of Radioanalytical and Nuclear Chemistry 249, 361-367.

Alyazichi, Y.M., Jones, B.G., McLean, E., Pease, J., Brown, H., 2017. Geochemical assessment of trace element pollution in surface sediments from the Georges River, Southern Sydney, Australia. Archives in Environmental Contamination and Toxicology 72, 247-259.

Azevedo, I., Ramos, S., Mucha, A.P., Bordalo, A.A., 2013. Applicability of ecological assessment tools for management decision-making: A case study from the Lima estuary (NW Portugal). Ocean and Coastal Management 72, 54-63.

Bull, A., Brown, M.T., Turner, A., 2017. Novel use of field-portable-XRF for the direct analysis of trace elements in marine macroalgae. Environmental Pollution 220, 228-233.

Cao, L.L., Huang, C.G., Wang, J.H., Xie, J., Ni, Z.X., Jin, G.X., Waxi, L.L., Chen, H.X., 2014. Pollution status of selected metals in surface sediments of the Pearl River estuary and Daya Bay, South China Sea. Journal of Residuals Science and Technology 11, 119-130.

Chaillou, G., Schäfer, J., Anschutz, P., Lavaux, G., Blanc, G., 2003. The behaviour of arsenic in muddy sediments of The Bay of Biscay (France). Geochimica et Cosmochimica Acta 67, 2993-3003.

Din, Z.B., 1992. Use of aluminium to normalize heavy-metal data from estuarine and coastal sediments of Straits of Melaka. Marine Pollution Bulletin 24, 484-491.

Ge, L., Lai, W., Zhou, S., Ren, J., Lin, L., Lin, Y., 2001. New XRF probe for in situ determination of concentration of multi-elements in ocean sediments. Chengdu Ligong Xueyuan Xuebao 28, 80–85.

Ge, L., Lai, W., Lin, Y., 2005. Influence of an correction for moisture in rocks, soils and sediments on in situ XRF analysis. X-ray Spectrometry 34, 28-34.

Higueras, P., Oyarzun, R., Iraizoz, J.M., Lorenzo, S., Esbrí, J.M., Martínez-Coronado, A., 2012. Low-cost geochemical surveys for environmental studies in developing countries: Testing a field portable XRF instrument under quasi-realistic conditions. Journal of Geochemical Exploration 113, 3-12.

Hubbell, J.H., Seltzer, S.M., 1996. X-ray mass attenuation coefficients. National Institute of Standards and Technology, Gaithersburg, Maryland.

Kennish, M.J., 1998. Trace metal-sediment dynamics in estuaries: Pollution assessment. Reviews in Environmental Contamination and Toxicology 155, 69-110.

636 Kirtray, V.J., Kellum, J.H., Apitz, S.E., 1998. Field-portable X-ray Fluorescence
637 Spectrometry for metals in marine sediments: Results from multiple sites. Water Science and
638 Technology 37, 141-148.
639
640 Lemiere, B., Laperche, V., Haouche, L., Auger, P., 2014. Portable XRF and wet materials:
641 application to dredged contaminated sediments from waterways. Geochemistry –
642 Exploration Environment Analysis 14, 257-264.
643
644 Loring, D.H., 1991. Normalization of heavy-metal data from estuarine and coastal
645 sediments. ICES Journal of Marine Science 48, 101–115.
646
647 Mejía-Piña, K.G., Huerta-Diaz, M.A., González-Yajimovich, O., 2017. Calibration of
648 handheld X-ray fluorescence(XRF) equipment for optimum determination of elemental
649 concentrations in sediment samples. Talanta 161, 359-367.
650
651 Mighanetara, K., Braungardt, C.B., Rieuwerts, J.S., Azizi, F., 2009. Contaminant fluxes
652 from point and diffuse sources from abandoned mines in the River Tamar catchment, UK.
653 Journal of Geochemical Exploration 100, 116-124.
654
655 Mucha, A.P., Vasconcelos, M.T.S.D., Boralo, A.A., 2004. Vertical distribution of the
656 macrobenthic community and its relationships to trace metals and natural sediment
657 characteristics in the lower Douro estuary, Portugal. Estuarine and Coastal Shelf Science 59,
658 663-673.
659

660 Nolting, R.F., Ramkema, A., Everaats, J.M., 1999. The geochemistry of Cu, Cd, Zn, Ni and
661 Pb in sediment cores from the continental slope of Banc d'Arquin (Mauritani). Continental
662 Shelf Research 19, 665-691.
663
664 Parsons, C., Grabulosa, E.M., Pili, E., Floor, G.H., Roman-Ross, G., Charlet, L., 2013.
665 Quantification of trace arsenic in soils by field-portable x-ray fluorescence spectrometry:
666 Considerations for sample preparation and measurement conditions. Journal of Hazardous
667 Materials 262, 1213-1222.
668
669 Quiroz-Jiménez , J.D., Roy, P.D., 2017. Evaluation of geochemical data by two different
670 XRF spectrometers in sediments from the Santiaguillo Basin (state of Durango, Mexico).
671 Geofíscia Internacional 56, 305-315.
672
673 Radu, T., Diamond, D., 2009. Comparison of soil pollution concentrations determined using
674 AAS and portable XRF techniques. Journal of Hazardous Materials 171, 1168–1171.
675
676 Rae, J.E., 1997. Trace metals in deposited intertidal sediments. In: Biogeochemistry of
677 Intertidal Sediments, ed. T.D. Jickells and J.E. Rae, Cambridge University Press, pp.16-41.
678
679 Regnier, P., Arndt, S., Goosens, N., Volta, C., Laruelle, G.G., Lauerwald, R., Hartmann, J.,
680 2014. Modelling estuarine biogeochemical dynamics: From the local to the global scale.
681 Aquatic Geochemistry 19, 591-626.
682
683 Roychoudhury, A.N., 2001. Dispersion in unconsolidated aquatic sediments. Estuarine,
684 Coastal and Shelf Science 53, 745-757.
685
686 Stallard, M.O., Apitz, S.E., Dooley, C.A., 1995. X-ray fluorescence spectrometry for field
687 analysis of metals in marine sediments. Marine Pollution Bulletin 31, 297-305.
688

689 Tjallingii, R., Röhl, U., Kölling, M., Bickert, T., 2007. Influence of the water content on x-
690 ray fluorescence core-scanning measurements in soft marine sediments. Geochemistry,
691 Geophysics, Geosystems 8, Q02004, doi:10.1029/2006GC001393.
692
693 Turner, A., 2010. Marine pollution from antifouling paint particles. Marine Pollution
694 Bulletin 60, 159-171.
695
696 Turner, A., 2017. In situ elemental characterisation of marine microplastics by portable
697 XRF. Marine Pollution Bulletin 124, 286-291.
698
699 Turner, A., Lewis, M., 2018. Lead and other heavy metals in soils impacted by exterior
700 legacy paint in residential areas of south west England. Science of the Total Environment
701 619-620, 1206-1213.
702
703 Turner, A., Millward, G.E., 2002. Suspended particles: Their role in estuarine
704 biogeochemical cycles. Estuarine Coastal and Shelf Science 55, 857-883.
705
706 Turner, A., Poon, H., Taylor, A., Brown, M.T., 2017. In situ determination of trace elements
707 in *Fucus* spp. by field-portable-XRF. Science of the Total Environment 2017, 593-594, 227-
708 235.
709
710 Wei, R., Haraguchi, H., 1999. Multielement determination of major-to-ultratrace elements in
711 river and marine sediment reference materials by inductively coupled plasma atomic
712 emission spectrometry and inductively coupled plasma mass spectrometry. Analytical
713 Sciences 15, 729-735.
714
715 Zhao, G., Ye, S., Yuan, H., Ding, X., Wang, J., 2017. Surface sediment properties and heavy
716 metal pollution assessment in the Pearl River Estuary, China. Environmental Science and
717 Pollution Research International 24, 2966-2979.

718